01 Feb 2008

Modeling of Trickle-Bed Reactors with Exothermic Reactions using Cell Network Approach

Jing Guo

Yi Jiang

Muthanna H. Al-Dahhan
Missouri University of Science and Technology, aldahhanm@mst.edu

Recommended Citation

J. Guo et al., "Modeling of Trickle-Bed Reactors with Exothermic Reactions using Cell Network Approach," *Chemical Engineering Science*, vol. 63, no. 3, pp. 751 - 764, Elsevier, Feb 2008.
The definitive version is available at https://doi.org/10.1016/j.ces.2007.09.050

ELSEVIER

Chemical Engineering Science 63 (2008) 751–764

Chemical Engineering Science

www.elsevier.com/locate/ces

Modeling of trickle-bed reactors with exothermic reactions using cell network approach

Jing Guo[a,*,1], Yi Jiang[b], Muthanna H. Al-Dahhan[a]

[a]*Chemical Reaction Engineering Laboratory, Department of Energy, Environmental and Chemical Engineering, Washington University, St. Louis, MO 63130, USA*

[b]*Corning Inc., One Science Center Road, SP-TD-01-1, Corning, NY 14831, USA*

Received 3 May 2007; received in revised form 24 September 2007; accepted 27 September 2007
Available online 10 October 2007

Abstract

One-dimensional (1D) and two-dimensional (2D) cell network models were developed to simulate the steady-state behavior of trickle-bed reactors employed for the highly exothermic hydrotreating of benzene. The multiphase mass transfer-reaction model and novel solution method are discussed in this report. The 1D model was shown to satisfactorily simulate the axial temperature field observed experimentally for multiphase flow with exothermic reactions. The 2D reactor modeling provided valuable information about local hot spot behavior within the multiphase reactor, identifying situations in which hot spots may form. The model took into consideration the heterogeneous nature of liquid distribution, including radial liquid maldistribution and partial external wetting. This approach was proven to be stable and efficient in dealing with the complex interaction of phase vaporization and temperature rise. Through analysis and discussion, this report established the cell network model as a valid representation of the flow environment produced in a trickle bed with exothermic reactions.

Keywords: Catalysis; Evaporation; Trickle bed reactors; Multi-phase flow; Reaction kinetics

1. Introduction

A large group of industrial processes involve exothermic catalytic reactions between liquid and gaseous components, such as hydrogenations and oxidations. One multiphase reactor frequently used in such industrial reactions is the trickle-bed reactor, in which gas and liquid flow downward through packed beds to undergo chemical reactions. During this process, reactor scale maldistribution and incomplete external wetting of particles can occur due to trickle flow. In large industrial units, considerable radial temperature gradients can exist when the reaction heat release and maldistribution of the liquid–gas mixture are significant. Unfortunately, mixing-cup temperature controls at the reactor outlet are not sufficient in preventing large temperature differences between the central zone of the packed bed and the wall (Specchia and Baldi, 1979). As a result, the interaction of heat and mass transfer during strong exothermic reactions inside the reactor can be so serious that under certain conditions, a partial or total phase change can occur. This may include an evaporation of the liquid phase, complicating both the reaction and transport phenomena. The higher reaction rate accelerates the heat production and thus enlarges the hot-spots. The result is the formation of hot zones that may have a deleterious impact on the yield of the desired product. For example, sintering of the catalyst has been observed in industrial trickle-bed reactors (Specchia and Baldi, 1979; Chaudhari et al., 2002; Deans and Lapidus, 1960). When a hot zone exists next to the reactors walls, there may be a decrease in the mechanical strength of the wall. This will eventually cause damage to the reactor vessel by generating a leak that may lead to an explosion. Thus, it is of great practical importance to understand the nature and origin of these hot spots and predict their location and size.

The hot zone evolution in a packed bed is affected by the integration of the reaction rate, transport of heat and species in the radial direction, and the impact on the fluid physical

* Corresponding author. Tel.: +1 3149354729.
E-mail address: jing.guo@uop.com (J. Guo).
[1] Currently affiliated with UOP LLC, Des Plaines, IL 60016, USA.

0009-2509/$ - see front matter © 2007 Elsevier Ltd. All rights reserved.
doi:10.1016/j.ces.2007.09.050

properties due to the changes of reactant concentrations and temperature in the flow direction. Considerable capital and operational costs have been invested to resolve rapid and excessive temperature changes. To reduce this cost and elucidate these phenomena, heterogeneous models have been developed. Remediation efforts have been made to provide a detailed analysis of non-isothermal effects on reactor operations, such as the one-dimensional (1D) reactor modeling and experiment verification reported for a trickle-bed reactor under non-isothermal conditions (Chaudhari et al., 2002). Two-dimensional (2D) models, including the cell network model, have been developed to locate the hot spot in the reactor.

The cell network model has come into being since the early 1960s. In its original concept, a packed bed of spheres was approximated as a cylindrically symmetrical network of perfectly stirred tank reactors. The reactants were envisioned to enter any given stirred tank as a single phase from the two preceding tanks. Alternative rows were offset at half a tank to allow for radial mixing. The effluent from the stirred tank was then fed through subsequent stages (Deans and Lapidus, 1960). Jaffe (1976) applied this concept to the heat release of a single phase hydrogenation process, and simulated the occurrence of steady state hot spots due to flow maldistribution. Schnitzlein and Hofmann (1987) developed an alternative cell network model in which the elementary unit consisted of an ideal mixer and a subsequent plug flow unit. These fluid streams were split or merged in infinitesimally small adiabatic mixing cells (without reaction), located between the different layers of the elementary units. Kufner and Hofmann (1990) incorporated the radial porosity distribution into the above cell model, which led to a better agreement of the predicted temperature profile with the experimental data. Despite all the development in the cell network model, one should note that the above-mentioned models were examined only for single phase flow with offset in alternative rows of cells.

In this work, our overall objective is to develop a model capable of handling multiphase flow and reactions, as well as temperature change due to both phase transition and flow maldistribution for a trickle-bed reactor. The model will serve as a guide to understanding the reactor performance and optimization. At first a comprehensive 1D mixing cell model is developed to account for the phase transition in pilot plant reactors devoid of radial flow maldistribution. This model includes the local changes of phase velocities, species concentrations, external wetting efficiency, liquid holdup and mass transfer rate due to phase transition, and their effects on the reaction rates. The 1D model is applied in the reaction system of benzene hydrogenation to cyclohexane in order to predict the temperature profiles and the change of species concentrations along the reactor axis. After the 1D model is validated against the experimental temperature data reported in the literature, it is extended to the 2D model to assess the impact of flow maldistribution on the formation of hot spots. The 2D model is able to take advantage of the validated 1D model and a new solution scheme is designed to expedite the solution process and to enhance the solution stability. The ultimate goal is to develop a reliable model that will enable a rational design and control to avoid the undesirable formation of hot spots.

2. 1D reactor model

2.1. Reactor scale model

The model is designed to incorporate exothermal reactions, vaporization of liquid phase components and the effect of partial external wetting of the catalyst. Plug flow for each phase is assumed in many reported reactor scale models that consist of a set of ordinary differential equations (ODEs) with well-defined initial and boundary conditions. However, when a large amount of heat is released due to chemical reactions, the numerical computation of these ODEs becomes difficult due to the stiffness of the equations. To overcome these difficulties we have implemented a cell network approach. As shown in Fig. 1, the reactor from the inlet to the outlet is divided into a number (N) of well-mixed cells in stacks along the axial direction. Mixing only occurs within each cell and backmixing is not accounted for between the adjacent cells. The grid independence was obtained after N reached a certain limit. The 1D model is applicable for systems without liquid or gas maldistribution.

Governing equations are presented for the multiphase mass transfer in each cell. The mass balance equations for any species in the reaction system need to be solved in conjunction with hydrodynamic and kinetic models. Mass transfer resistances consist of the resistance between the gas, liquid and solid phase, whereas the intraparticle mass transfer is reflected by the catalyst effectiveness factor. An external wetting efficiency (η_{CE}) was introduced in the cell model to account for the partial external wetting of the catalyst particles in the local cell. The mass balance equation for liquid phase at each cell is given as

$$U_L \frac{(C_{k,L} - \phi_{k,L})}{L_c} = (K_L a_{GL})_k [C_{k,e} - C_{k,L}] - k_{LS,k} a_{LS} [C_{k,L} - C_{k,LS}]. \quad (1)$$

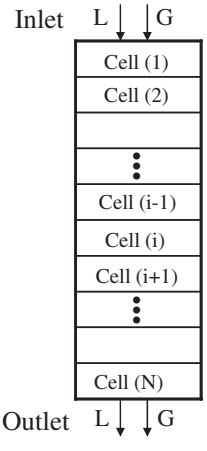

Fig. 1. Schematic representation of flow through the cell stacks.

Mass transfer between liquid phase and solid catalyst

$$k_{LS,k}a_{LS}[C_{k,L} - C_{k,LS}] = (1-\varepsilon_B)\eta_{CE}\eta_o \cdot v_k(-r_L). \quad (2)$$

Boundary conditions

$$C_{k,L} = \phi_{k,L}|_{z=0}, \quad (3)$$

where

$$\frac{1}{(K_L a_{GL})_k} = \frac{1}{k_L a_{GL}} + \frac{1}{\mathrm{He}_k k_G a_{GL}}. \quad (4)$$

The amount of mass exchange can be predicted by the product of the overall liquid–gas mass transfer coefficient $(K_L a_{GL})_k$ and the driving force between the hypothetical concentration of liquid in equilibrium with bulk gas species $(C_{k,e})$ and the species concentration in liquid bulk $(C_{k,L})$ (Levenspiel, 1996). k_L and k_G are the mass transfer coefficients in the liquid side and gas side, respectively. L_c is the axial length of each cell. For any given set of inlet conditions, the catalyst effectiveness factor, temperature, species concentrations and the variations in volumetric flow due to gas-phase reactions are calculated at each cell.

The generalized governing equation for gas phase at each cell can be described as

$$\frac{1}{L_c}(U_{G,\mathrm{out}}C_{k,G} - U_{G,\mathrm{in}}\phi_{k,G}) = -(K_L a_{GL})_k[C_{k,e} - C_{k,L}] - k_{GS,k}a_{GS}[C_{k,e} - C_{k,GS}]. \quad (5)$$

Mass transfer

$$k_{GS,k}a_{GS}[C_{k,e} - C_{k,GS}] = (1-\varepsilon_B)(1-\eta_{CE}) \cdot v_k(-R_G). \quad (6)$$

Boundary conditions

$$C_{k,G} = \phi_{k,G}|_{z=0}. \quad (7)$$

In the governing equations, liquid phase concentration $C_{k,L}$ and gas phase concentration $C_{k,G}$ are for species k inside the cell and at cell outlet, because the cell is operated as a stirred tank. $\phi_{k,L}$ and $\phi_{k,G}$ represents the feed concentrations of liquid and gas from the previous cell for species k.

The effects of heat necessitate the simultaneous consideration of heat and component material balances for the external field at the same time. A reaction rate expression depending on both temperature and concentration appears directly in all the balances. Energy balance is considered for the whole cell to get the local cell temperature. It is assumed that inside the particles the heat transfer is fast enough and temperature gradients are small enough, so that the solid temperature is considered equal to the gas and liquid temperature in each cell. The energy balance for each cell in the reactor can be expressed as

Accumulation of fluid enthalpy
= reaction heat − heat consumed for evaporation
− heat loss to wall, (8)

$$\frac{1}{L_c}[U_L\rho_L c_{p,L}(T-\psi) + (U_G\rho_G)_{\mathrm{out}}c_{p,G}T - (U_G\rho_G)_{\mathrm{in}}c_{p,G}\psi] = [(-\Delta H_R)_L\eta_{CE}\eta_o(1-\varepsilon_B)(-r_L) + (-\Delta H_R)_G(1-\varepsilon_B)(1-\eta_{CE})\cdot(-R_G)] - \sum_k(\Delta H_v)_k\{-(K_L a_{GL})_k(C_{k,e} - C_{k,L}) - k_{GS,k}a_{GS}[C_{k,e} - C_{k,GS}]\} - \frac{Q_w}{V_c}. \quad (9)$$

The heat released during the reaction is carried away by the bulk liquid and gas phases, evaporation of the liquid phase and heat transfer from the cell to the reactor wall, which is represented by the bed-to-wall heat loss, Q_w:

$$Q_w = U_w A_w (T - T_w). \quad (10)$$

2.2. Determination of physical properties and parameters

The reaction system contains hydrogen (gas) and benzene/cyclohexane mixture (liquid). Physical properties that are needed for the model are taken from the Chemical Properties Handbook (Yaws, 1999), such as the standard enthalpy of gas compound formation at standard temperature of 298.15 K, i.e., $\Delta H_{f,G}$. If species resumes gas phase at operating temperature T, then $\Delta H_{f,G}$ serves as the basis for enthalpy calculation.

$$\Delta H_{298.15} = \Delta H_{f,G}. \quad (11)$$

Otherwise, if the species is in a liquid state at T, then the basis is enthalpy of formation of the liquid at 298.15 K.

$$\Delta H_{298.15} = \Delta H_{f,G} - \Delta H_v^0. \quad (12)$$

ΔH_v^0 is the enthalpy of vaporization at standard temperature of 298.15 K. Now that the species enthalpy of formation at 298.15 K is available, its value at given temperature T is gained from integration (13).

$$\Delta H_T = \Delta H_{298.15} + \int_{298.15}^{T} c_p \,\mathrm{d}t, \quad (13)$$

where c_p is a function of temperature, $c_p = a_1 + a_2T + a_3T^2 + a_4T^3 + a_5T^4$, as the assumption of constant heat capacity is questionable for gas phase in which large temperature variations occur within the bed. The integral leads to

$$\Delta H_T = \Delta H_{298.15} + \left[\left(a_1 + \frac{a_2}{2}T + \frac{a_3}{3}T^2 + \frac{a_4}{4}T^3 + \frac{a_5}{5}T^4\right)T - \left(a_1 + \frac{a_2}{2}T_0 + \frac{a_3}{3}T_0^2 + \frac{a_4}{4}T_0^3 + \frac{a_5}{5}T_0^4\right)T_0\right], \quad (14)$$

where $T_0 = 298.15$ K.

Henry's law constant (He) for hydrogen (species 1) is calculated as

$$He_1 = \frac{C_{1,G}}{C_{1,e}}, \quad (15)$$

where the solubility of hydrogen $(C_{1,e})$ in the solvent, cyclohexane, was reported as (Ronze et al., 2002)

$$\log 10(C_{1,e}RT/\mathrm{MPa}) = 363.84/T + 1.1809. \quad (16)$$

Henry's law constant for other species k ($k \neq 1$) are connected to their vaporization pressure and calculated as (Perry and Green, 1997)

$$He_k = \frac{C_{k,G}}{C_{k,e}} = \frac{P_{k,v}}{RTC_{\text{total},L}}. \tag{17}$$

The vaporization of the vapor pressure with temperature for species k was calculated from the equations reported in the literature (Levenspiel, 1996)

$$\log 10(P_{k,v}/\text{mmHg}) = A + B/T + C \cdot \log 10(T) + D \cdot T + ET^2. \tag{18}$$

Because of the mass transfer to the gas from the flowing liquid film and the static liquid inside the catalyst pore, the total molar gas flux undergoes changes and the gas velocity has to be updated from cell inlet to outlet. The variation in gas velocity is accounted for as follows:

$$U_{G,\text{out}} = U_{G,\text{in}} \left(\frac{P_{\text{in}}}{P_{\text{out}}} \right) + (F_{G,\text{out}} - F_{G,\text{in}}) \cdot \frac{RT}{P_{\text{out}}}, \tag{19}$$

where the two-phase pressure drop in one cell is calculated explicitly from the correlation reported by Ramachandran and Chaudhari (1983). In order to account for possible pressure losses due to sufficiently long reactor and small reactor void, pressure drop calculation is necessary.

The correlations reported in the literature are adopted to calculate the model parameters. Convective mass transfer coefficient in the liquid side, k_L, is evaluated using the correlation of Fukushima and Kusaka (1977). Convective mass transfer coefficient in the gas side, k_G, is evaluated according to the correlation for gas–solid mass transfer coefficient, k_{GS} (Dwivedi and Upadhyah, 1977). The liquid–solid mass transfer coefficient, k_{LS}, is estimated by the correlation of Tan and Smith (1980). The dynamic liquid holdup and static liquid hold up are calculated using the model of Ellman et al. (1990) and Mao et al. (1993) for trickle beds, respectively. The bed-to-wall heat transfer coefficient, U_w, is evaluated from the correlation of Specchia and Baldi (1979). The effective diffusion coefficient of species in the liquid phase is involved in the above correlations and can be computed from molecular diffusion coefficient using the porosity of the catalyst pellet ($\varepsilon_p = 0.5$) and the tortuosity factor ($\tau = 4$). The molecular diffusivity of hydrogen in benzene/cyclohexane mixture ($D_{m,1}$) was evaluated from the correlation of Snijder et al. (1994):

$$D_{m,1} = 4.780 \times 10^{-4} \text{e}^{-3239/T}. \tag{20}$$

Catalyst pellets are described in the form of 1D slab with both sides exposed to either gas or liquid. For the down flow operation, catalyst pellets are divided into three liquid–solid contacting categories: (a) both catalyst surfaces are completely wetted (liquid covered); (b) one of the catalyst surfaces is wetted and the other one is dry; and (c) both catalyst surfaces are completely dry (gas-covered). The fraction of the external catalyst surface that is actively covered with liquid is η_{CE}. The wetted catalyst pellets completely covered by liquid are internally wetted because of the capillary forces, and all species diffuses in the particles via the liquid phase. In contrast, The externally gas-covered catalyst pellets are assumed to be internally completely dry, and the diffusion of all species occurs in the gas phase inside the particles. The catalysts with half external surface wetted are assumed to be half internally wetted because of the equilibrium between the liquid diffusion from the liquid external film into the catalyst pore and liquid vaporization from the catalyst pore through the catalyst dry surface.

For the fully wetted and partially wetted particles, i.e., categories (a) and (c), the species concentrations over the wetted catalyst surface are assumed to be the same and can be calculated from the liquid phase governing equations. Similarly, the species over the actively dry catalyst surface can be derived from the governing equations for gas phase. The external catalyst wetting efficiency, η_{CE}, is obtained from the El-Hisnawi's correlation (Guo and Al-Dahhan, 2004) as a function of $Re_L^{0.146}$. Since η_{CE} depends on the liquid mass flux into the control cell, its value changes from cell to cell along the reactor axis with the variations of liquid velocity and density due to the loss of liquid components into the vapor. For the cells receiving no liquid mass flux, the wetting efficiency is set as 0.

2.3. Reaction kinetics

Benzene hydrogenation to cyclohexane on the amorphous catalyst of Ni–B alloy over Al_2O_3 is expressed as

$$3H_2 + C_6H_6 \rightarrow C_6H_{12} + 216.12\,\text{kJ/mol}. \tag{21}$$

Reaction heat is calculated at 500 K for the above reactions. The side reactions include hydrocracking with carbon and methane as the final products, hydroisomerization, and full saturation of benzene to methane. Since this work is focused on the application of a cell network model approach, the side reactions are assumed negligible under the investigated temperature range to simplify the theoretical analysis. The intrinsic reaction rate of benzene in the liquid phase is expressed as (Zhou et al., 2005)

$$r_L = k_{p0} \text{e}^{-43\,880/RT} P_1. \tag{22}$$

Considering the large catalyst pellet used in the reactor and the low ratio of the catalyst surface area to the gas–liquid interfacial area, the internal diffusion is depicted by the effectiveness factor for the spherical catalyst covered by liquid film (Zhou et al., 2005):

$$\eta_0 = \frac{1}{M_T} \left[\frac{1}{th(3M_T)} - \frac{1}{3M_T} \right], \tag{23}$$

where

$$M_T = \frac{d_p}{6} \sqrt{\frac{k_w \rho_p}{D_{\text{eff}}}}. \tag{24}$$

The hydrogenation rate of benzene in a gas phase within a dry catalyst pore was given as the Langmuir–Hinshelwood

expressions (Zhou et al., 2005). The denominator of such kinetic expression consists of the adsorption–desorption terms.

$$R_G = \frac{k_{p1} e^{-28\,250/RT} P_2 P_1^{0.5}}{[1+1.80\times10^{-4} e^{41\,170RT} P_2][1+2.95\times10^{-2} e^{-9370/RT} P_1^{0.5}]} \quad \text{for } T < 483\,\text{K}, \tag{25}$$

$$R_G = \frac{k_{p2} e^{-18\,612/RT} P_2 P_1^{0.5}}{[1+1.80\times10^{-4} e^{41\,170/RT} P_2][1+2.95\times10^{-2} e^{-9370/RT} P_1^{0.5}]} \quad \text{for } T > 483\,\text{K}. \tag{26}$$

In this work, values of activation energy ΔE and prefactor for the adsorption equilibrium constants were selected as reported above, as well as values of activation energy E for reaction rate constants. However, the Arrhenius prefactors (k_{p0}, k_{p1}, k_{p2}) for reactor rate constants were optimized by fitting the temperature profiles derived from 1D simulation in this work with the experimental data reported by other researchers (Cheng et al., 2001; Cheng and Yuan, 2002). The selected experimental data was based on three operating conditions. After the Arrhenius prefactors were chosen from fitting experimental data obtained on one condition, they were applied unchanged for the remaining two conditions. It is worth noting that, even after the values of Arrhenius prefactor are optimized, the corresponding reaction rate constants remain as the function of temperature and would vary with the temperature rise. The aforementioned approach is reasonable given that our goal is to develop a better qualitative understanding of the effects of various process parameters on observed trends of temperature rise in exothermic reaction system. Such an understanding is essential to incorporate the kinetics model into the reactor model and to refine the reactor model for better predictive ability.

In the experiments (Cheng et al., 2001; Cheng and Yuan, 2002), the stainless steel reactor had a wall thickness of 2.5 mm, length of 1.6 m, and inside diameter of 20 mm. The reactor wall was wrapped with an electrical heating band. The amorphous Ni–B alloy catalysts were 3 mm in diameter, and were packed to a height of 1.0 m between two inert packing layers on both ends, in order to provide uniform distribution and saturation of the reaction mixture by hydrogen. Under the reported experimental conditions, the maximum concentration difference of benzene between the bulk of the gas and the catalyst surface was estimated to be lower than one percent of the benzene concentration in the bulk phase. Thus, the concentration between the gas bulk and the particle surface were assumed negligible (Zhou et al., 2005).

3. Results and discussion of 1D model

The reactor was divided into a group ($N = 200$) of cells from inlet to outlet. The local variables at each cell, including component concentrations, temperatures, and velocities, were computed numerically. On the basis of the orthogonal collocation method, the code was programmed in FORTRAN language. Elementary object oriented programs were set up through the use of data structures. The data structure was composed to describe each cell with all physical and thermal properties defined as the structural elements. The program provided the modules a means to assess the changes in operating conditions and corresponding parameters.

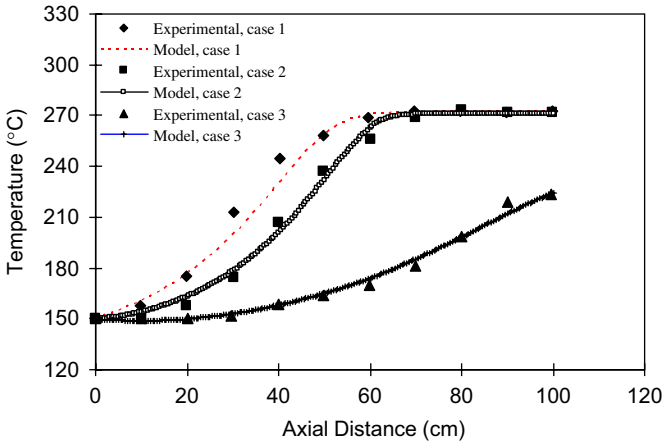

Fig. 2. Experimental observation reported in the literature (Cheng and Yuan, 2002; Watson and Harold, 1993) and model prediction of reactor performance under three given conditions. $P = 1.0$ MPa; $T_{in} = T_w = 150\,^{\circ}$C. *Case* 1: $C_B^0 = 31.5\%$, $L = 1.1\,\text{kg/m}^2\,\text{s}$, $G = 15.5\,\text{nL/min}$; *case* 2: $C_B^0 = 23.8\%$, $L = 1.3\,\text{kg/m}^2\,\text{s}$, $G = 15.4\,\text{nL/min}$; *case* 3: $C_B^0 = 23.8\%$, $L = 4.1\,\text{kg/m}^2\,\text{s}$, $G = 15.4\,\text{nL/min}$.

In order to compare the experimental data with the model prediction, the governing equations were solved numerically to obtain exit concentrations of benzene, and the temperate along the axis under the experimental conditions. Fig. 2 shows the simulated (lines) and experimental (discrete dots) temperature profiles for the three different operating conditions, as listed in Table 1. It should be noted that the pre-exponential factors of the kinetic constants were adjusted to obtain the fits of experimental data in case 2 and then used for cases 1 and 3.

The energy acquired from the reaction heat can be immediately absorbed through evaporation, and hence the temperature profile is rather flat near the reactor inlet. This denotes that the catalyst particle is covered by liquid. A negligible effect of benzene concentration on the temperature profile in this regime is observed due to the existence of the large excess of benzene in the liquid phase. In this situation the reaction rate is dominated by hydrogen pressure in view of its limited solubility in cyclohexane. After a certain length the temperature was found to increase rapidly in the low liquid flow rate of 1.1 and 1.3 $\text{kg/m}^2\,\text{s}$. With some liquid evaporation, the catalyst's external surface is partially dried and the gaseous hydrogen has more access to the catalyst pore. This is beneficial for facilitating the transport process of gas reactant due to the direct mass transfer of gas phase reactant to the catalyst surface. When more catalyst pores get exposed to the gas phase, the stepwise increment in the reaction rate takes place. Ineffective heat removal associated with the gaseous system and the absence of a local vaporization process also contributed to the higher rate. The presence of a phase transition was supported by the fact that the boiling point of the benzene/cyclohexane mixture is 180 °C at 1.0 MPa (Cheng et al., 2001). Hence, the liquid in the bulk phase did not exist above this temperature in the second half of the reactor, although part of liquid in the catalyst

Table 1
Operating conditions used in experiments and simulations

	Pressure (MPa)	Inlet and wall temperature (°C)	Inlet benzene volume fraction (%)	Liquid flux (kg/m^2 s)	Gas flow rate (nL/min)
Case 1	1.0	150	31.5	1.1	15.5
Case 2	1.0	150	23.8	1.3	15.4
Case 3	1.0	150	23.8	4.1	15.4

pores may still exist for higher temperatures due to the capillary effect. Further downstream, the variation in temperature with an inlet feed concentration indicated that the reaction rate was a function of benzene concentration. This implies that the reaction mainly occurs regionally during the gas phase. Near the end of the reactor for the low liquid flow rate, the reactant concentration became much lower and the reaction rate drops. The temperature profile finally flattens out. As the inlet liquid mass flux decreases, the catalyst layer required for the full liquid evaporation gets shorter, and the zone before sharp temperature increase becomes shorter. In contrast, with high liquid rate of 4.1 kg/m^2 s, the temperature rose slowly and most part of the reactor was operated below 180 °C. This means that the reaction is carried out under the full liquid condition.

Not only can the simulated profiles qualitatively capture the above-mentioned trend of the experimental temperature profile, but the model simulation also matches the actual value of the measured temperature profiles. A strong agreement between the experiments and the model predictions indicates the applicability of the mathematical model for the reactor over a range of conditions. By considering the interaction between cells along the axial direction, the cell stacks create a 1D model that is suitable for the interpretation of bench scale and pilot scale data over a range of conditions. Such a 1D structure provides the ground to expand the model to 2D by choosing an empirical radial mixing rule for the adjacent cells. The 2D model then allows the prediction of the performance of a reactor subject to either a uniform distribution or a gross maldistribution of each phase. A number of diverse reactor models can be obtained by simply choosing a scheme for connecting the cells.

4. 2D reactor model

4.1. Connection between 1D and 2D models

The development of the 1D reactive flow models have set up a solid foundation for their expansion to 2D models. The 1D structure with one inlet and one outlet can serve as a building element (cell) with suitable modifications. The 2D discrete cell network concept was developed so that the flow distribution in multiphase packed-bed reactors can be implemented in a realistic way. For the 2D simulation, a continuously stirred tank, as represented in Fig. 3a, is employed for each cell. Actually, for any specific cell, there are four possible types of flow stream distributions. Type-1 has one inlet and three outlets, Types-2 and 3 have two inlets and two outlets, but with opposite radial flow directions and Type-4 has three inlets and one outlet. This way any cell can be classified into one of these four categories. However, for computational purposes, each type can have inlet streams mixed before they enter into the cell, and have a single outlet stream split up after leaving the cell. Without undermining the physical configuration of each type, we can formulate the equivalent cell configuration with the mixing and splitting schemes as shown in Fig. 3b. This way the robustness and reliability of the established 1D model with one inlet and one outlet is resumed. In fact, the 2D scheme can be easily extended to a 3D scheme by adding two more streams along the third direction. All mass and energy balances are still solved in one cell only. The additional simulation code required for accomplishing the expansion from a 1D to 2D or 3D model is just a program for the mixing at the cell inlet and splitting at the outlet.

4.2. Solution scheme for 2D model

A novel approach was applied to solving the 2D mixing cell network model. Since a given cell is not affected by fields downstream, the calculation to the complete set of equations proceeds sequentially starting from the inlet row of cells. Then the solution can be accomplished layer by layer due to the initial value nature of the problem. Inlet conditions for flow velocities and species concentration were given at the first layer of cells. Wall temperature is assigned to cells adjacent to the wall, and fluid velocities are set to 0 at the wall side of these cells.

Within each layer, the cells were solved following a certain sequence. As shown in Fig. 4, the program initially swept from one side to the other at any given layer, and located the cells which were ready to be resolved, i.e., only one inlet from the previous layer which has known values of velocities and concentrations (Type-1 aforementioned). The developed 1D program was adopted to solve this particular cell. Its outlet stream properties, including species concentrations and flow properties, were obtained. The outlet stream was split into three branches, and each of them carried the same fluid properties (temperature and species concentration). The radial velocities assumed the specified values and the axial outlet velocity was calculated based on the phase mass balance. The flag was labeled to such cell as “solved”. In the second round sweep, the program located cells that have two stream inlets (Type-2 or Type-3), with one of the stream inlets calculated during the first round sweep and the other inlet coming from the resolved layer located above. Once this cell was located, these two stream inlets were mixed, and the mixture properties were obtained before they entered into a cell as one mixed stream inlet. The developed 1D program was then employed to solve for the variables at this cell. The two outlet streams possessed

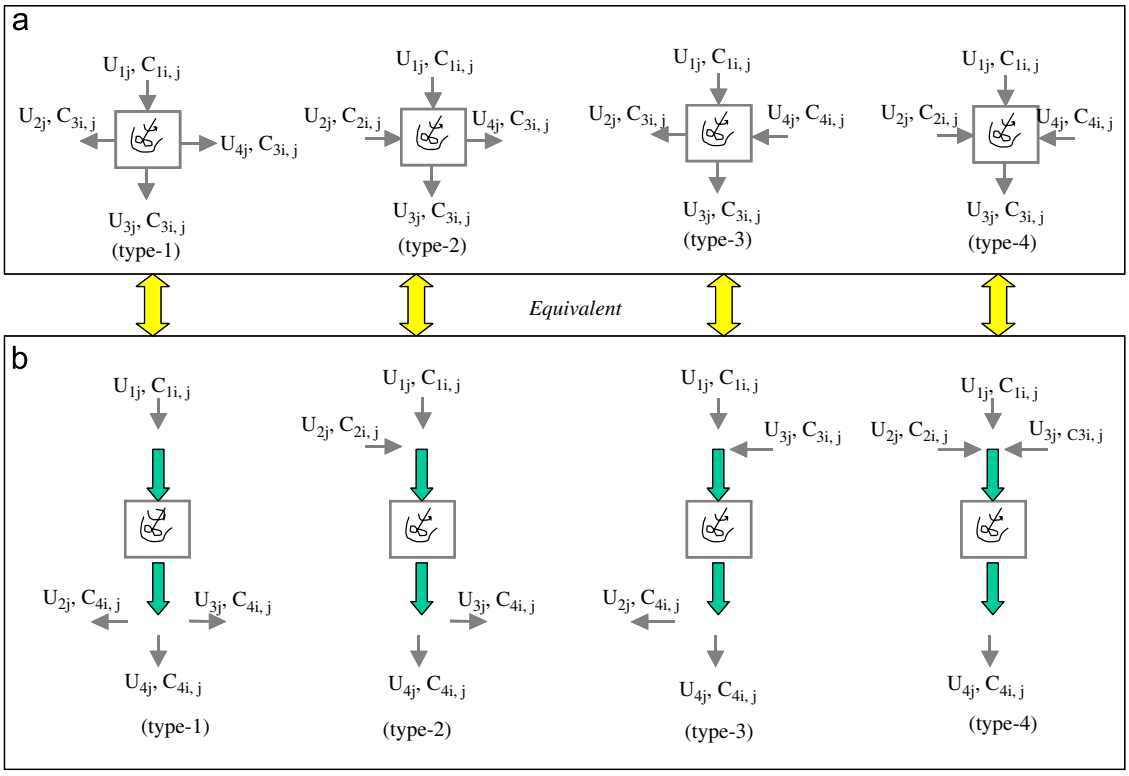

Fig. 3. Connections between 2D and 1D models.

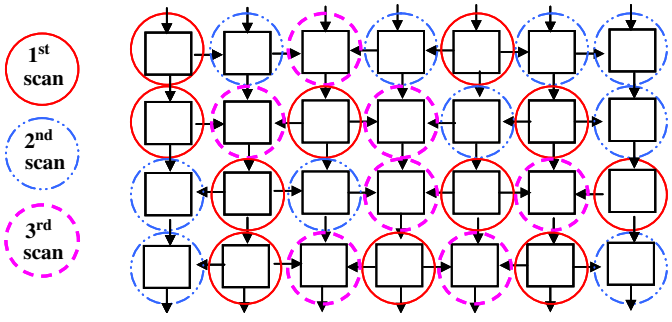

Fig. 4. Two-dimensional interconnected cell network and proposed solution scheme.

the same fluid properties, and the axial outlet velocity was calculated based on the phase mass balance since the radial outlet velocity was specified in advance. Such cell was labeled as "solved". During the final round of sweep, the program found cells that had three stream inlets (Type-4). Two of the radial streams were then established after the previous two rounds of sweeps, the third axial inlet was known since it came from the layer above. These three streams were mixed to create one mixture stream inlet to the cell. Once the 1D program was used to solve for the only axial outlet stream, this cell was marked as "solved". These three rounds of sweep were designed to solve all types of cells in one layer. The convergence and stability of the numerical calculation in each cell could be tracked and analyzed. The numerical difficulty, if existing in one specific cell, could be easily diagnosed and fixed. After the label of every cell in this layer was confirmed as "solved", the program started working on the next layer.

When one cell became solvable with all inlet variables known, first the parameters (local wetting contact fraction, mass transfer coefficients, hydrodynamics, etc.) and the reaction rates were obtained by using separate modules. The information gathered from these modules was then coupled with the material balance function so that the molar flow rates of all components were computed. Finally, the gas velocity was corrected for volumetric expansion. The values at the exit of each given control volume were used as input values to the adjacent control volume. It should be noted that overall heat transfer from the bulk liquid phase to the reactor was accounted for. The heat loss to the wall was assessed only for the first and last cells in each layer. For other cells that are not near the wall, adiabatic conditions were assumed and the term Q_w in Eq. (9) is neglected.

The mass transfer-reaction interaction is tackled in one cell. In fact, the code has been designed to accommodate a number of reactions, regardless of their heat release level. This feature of the cell model is especially useful for the petrochemical and aromatics reaction system, where the complex kinetics and enormous reaction heat may be difficult for the other models to handle. The heat and material balances for a cell in the model were reduced to purely algebraic form in the steady state with initial-value nature. This process offers numerous mathematical advantages over the techniques required to solve the 2D boundary-value problems in partial differential equations. Due to the sequential approach of the finite cell model,

convergence was only to be obtained at one geometric position at a time. However, in the boundary value problem represented by the differential-balance model an iteration scheme would have to be applied simultaneously at all positions in the bed. In that case, the rate of convergence is usually much slower, even if the initial guess at all points is good enough for eventual convergence to occur.

5. Results and discussion of 2D model

The coupling between hydrodynamics and the chemical reactions is two-way. Due to the phase change and temperature effect, the flow rates and species concentration profiles were affected. This in turn impacted the local reaction rate, heat release and evaporation rate. In addition, the maldistribution of the liquid and gas in the reactor across its diameter could lead to a simultaneous occurrence of reaction on the completely wetted, partially wetted and non-wetted catalyst pellets. To improve the understanding of the hot spot formation, various factors, including inlet flow rates and radial velocity, need to be studied. The geometry in all cases has 200 axial sections, and 13 radial sections. The operating conditions of case 2 given in Table 1 are used for all cases. For each case, the cell configuration and maldistribution conditions are given, followed by both the temperature and concentration profiles.

5.1. Base case

Distribution of cell section and feed velocity in the 2D model is depicted in Fig. 5, where no radial flow is considered. In fact, the cell in each radial section is similar to the previous 1D case, except that the cell radial cross sectional area is smaller and the heat loss to the reactor wall is considered only in radial section 1 and 13, which are cells adjacent to the reactor wall. The ignorance of the radial flow and heat conduction inside the reactor, although non-physical, is beneficial to validate the model expansion from 1D geometry to 2D by confirming that the values of exit radial temperature in this case match the exit temperature value predicted in the 1D case.

The 2D temperature distribution inside the reactor is given in Fig. 6a. The radial direction temperature is uniform except in the zone nearby the reactor wall, where there is actual heat loss to the wall. The temperature hardly rises in the entry section of the reactor. The catalyst is contacted by a thin liquid film containing the sparingly soluble hydrogen. Liquid components gradually vaporize with the progress of the chemical reaction. The bulk liquid film external to the catalyst disappears if the local temperature exceeds the liquid mixture bubble point. After a sufficient time lapse, a fraction of catalyst becomes exposed to the gas. A more rapid gas phase catalytic reaction occurs with an accompanying temperature excursion. As the gas diffusion is several orders of magnitude higher when compared to that in the liquid under conditions of partial wetting, it is expected

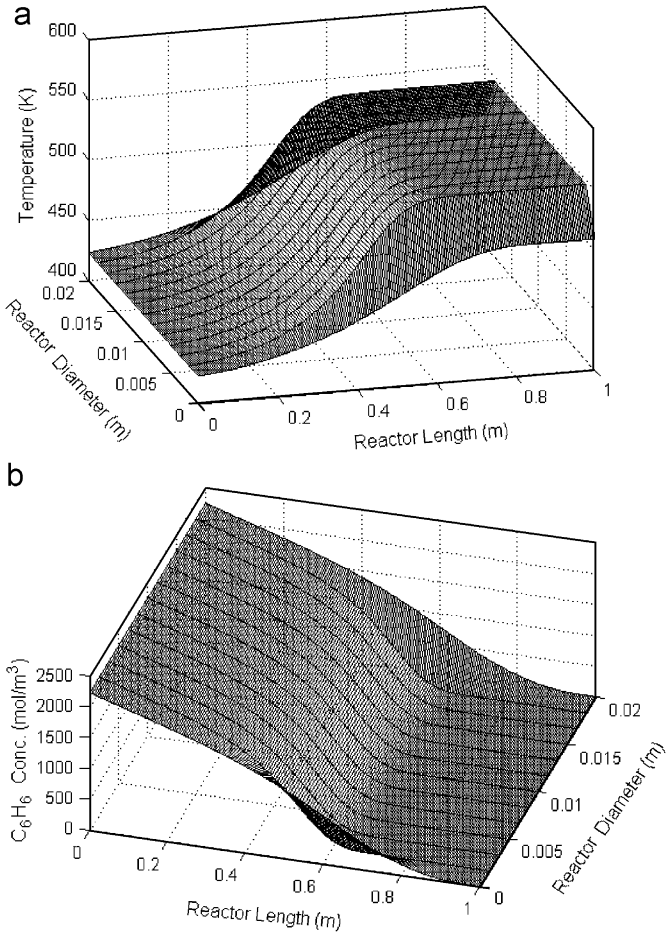

Fig. 6. Distribution of temperature rise (a) and benzene concentration (b) in 2D model, no radial flow distribution. Reaction conditions as given in case 2: $P = 1.0\,\text{MPa}$, $T_{\text{in}} = T_w = 150\,^{\circ}\text{C}$, $C_B^0 = 23.8\%$, $L = 1.32\,\text{kg/m}^2\,\text{s}$, $G = 15.4\,\text{nL/min}$.

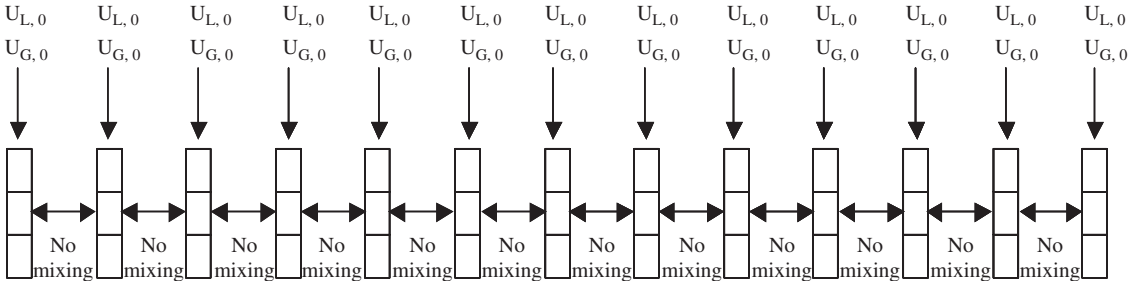

Fig. 5. Distribution of cell section and feed velocity in 2D model, no radial flow distribution. Reaction conditions given in case 2: $N = 13$ cells, $P = 1.0\,\text{MPa}$, $T_{\text{in}} = T_w = 150\,^{\circ}\text{C}$, $C_B^0 = 23.8\%$, $L = 1.32\,\text{kg/m}^2\,\text{s}$, $G = 15.4\,\text{nL/min}$.

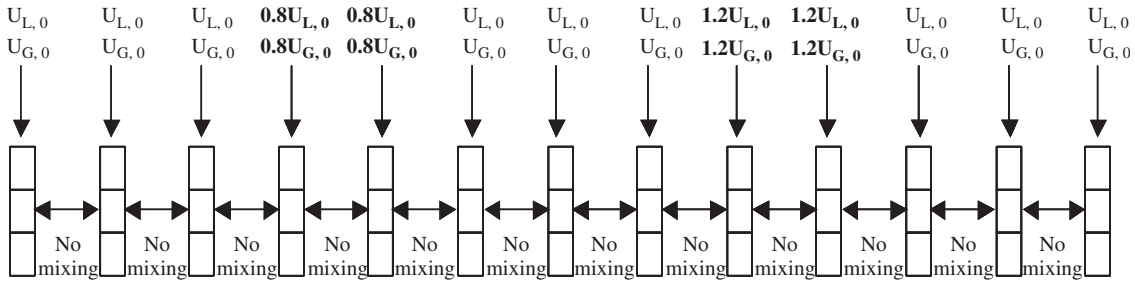

Fig. 7. Unevenly distributed feed rate at reactor inlet, with same ratio of $U_{L,0}/U_{G,0}$ at every inlet cell. No radial flow distribution. Reaction conditions as given in case 2. Thirteen radial cell columns.

to show a higher rate of reaction, which in turn accelerates the pore emptying process by providing an effective source of energy in the immediate vicinity of the liquid front (Watson and Harold, 1993). Eventually, the liquid front recedes a sufficient distance into the pellet. The drying rate drops sharply until the pellet is lacking in liquid. During sufficiently long periods when the pellet becomes nearly devoid of liquid, the liquid in the inner core and small pores is then vaporized. The imbalanced rates of energy consumption by vaporization and of energy supply from reaction heat continue until the point where the temperature at the cell reaches its maximum value. At high temperatures reactants are exhausted, as seen in Fig. 6b, and the predicted reaction and heat generation cease. Since the reactant conversion differs greatly due to the occurrence of phase transition, phase transition is a favorable operating mode in achieving a higher reactant conversion. This maximizes the utilization of the reactor volume. Intriguingly, controlled hot spot formation by periodic on-off liquid flow may result in substantially higher conversions compared to the continuous uniform liquid flow (Haure et al., 1989).

5.2. *Perturbed inlet flow rates with constant liquid–gas velocity ratio*

Injection position and flow rate of the inlet fluids are two variables that need to be studied to understand their effects on the maximum temperature rise and benzene conversion. Instead of modifying the entire inlet, only a region of low flow rate ($0.8U_{L,0}$, $0.8U_{G,0}$) and high flow rate ($1.2U_{L,0}$, $1.2U_{G,0}$) were taken into consideration. Beyond these two regions, the inlet conditions were unaffected, as displayed in Fig. 7. Both liquid and gas phases assumed low flow rates in the two specified radial sections 4 and 5. In contrast, both a high flow of liquid and gas with high flow rates are injected at two specified right sections 9 and 10. The velocity profile was chosen to maintain the overall mass flow rates of gas and liquid through the reactor cross sectional area. In addition, the liquid–gas mass flow ratio is kept constant for every section. No radial velocity was considered in this case.

The dynamic liquid holdup is directly proportional to the ratio of the liquid mass flow rate to the gas mass flow rate, and hence to their ratio of velocity if the phase density is constant (Ellman et al., 1990). On the other hand, the external wetting

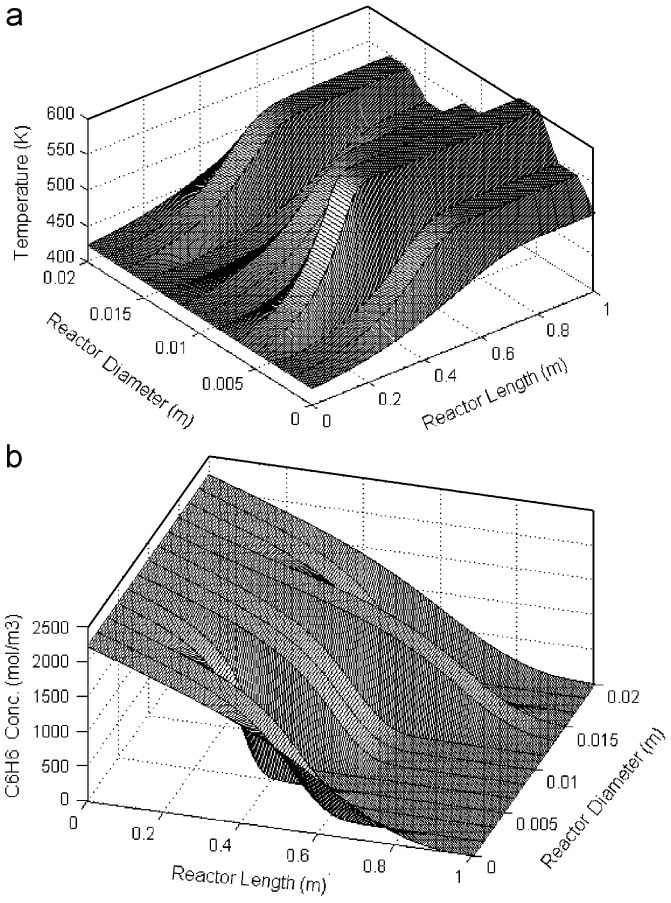

Fig. 8. 2D temperature profile (a) and benzene concentration profile (b). Unevenly distributed feed rate at reactor inlet, with same ratio of $U_{L,0}/U_{G,0}$ at every inlet cell. No radial flow distribution.

efficiency is exclusively dependent on the liquid mass flow (Snijder et al., 1994). Based on the selected inlet conditions, the dynamic liquid holdup was not changed throughout the whole reactor. The lower wetting efficiency in the low liquid flow ($0.8U_{L,0}$) led to more catalyst surface exposure to the gas phase, and a higher reaction rate. As a consequence, the maximum temperature was also increased. The predicted profile reveals that the injection of a low flow rate would lead to a temperature rise as high as 177 K, as shown in Fig. 8a. The regime through which the catalysts become fully dry is shortened

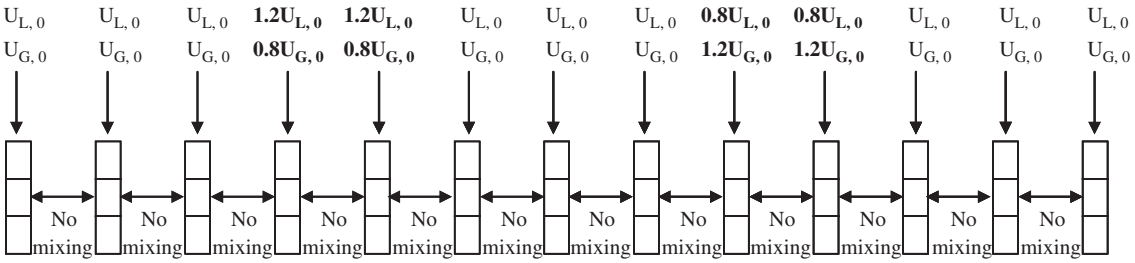

Fig. 9. Unevenly distributed feed rate at reactor inlet, with varied ratio of $U_{L,0}/U_{G,0}$ at specified inlet locations. No radial flow distribution. Reaction conditions as given in case 2. Thirteen radial cell columns.

with a decreasing liquid flow rate. The corresponding higher conversion level in the low liquid flow section is shown in Fig. 8b. Within the hottest zones the pellets are completely dry, and catalysis proceeds on gas-contacted catalyst surfaces. For the sections with high liquid velocities ($1.2U_{L,0}$), an increase in the wetted fraction retards the reaction rate, overcoming the opposite effect of the increased external mass transfer rate. In addition, the reaction heat release is removed at a significantly higher rate with higher liquid velocity. Hence, the temperature rise decreases with an increase in liquid flow rate. In the coolest zones of the reactor, the pellets are likely to be filled with liquid because of strong capillary forces. Reaction proceeds via liquid-phase catalysis. The slow rise of reaction temperature and the increased throughput of benzene are the major reasons for the drop of the conversion with increasing liquid flow rate, as shown in Fig. 8b. It is evident that the low flow rate of liquid and the resulting lower liquid–solid contact, provided that liquid–gas ratio remains constant, could lead to a hot spot where the temperature is much higher than the surrounding zones.

5.3. Perturbed inlet flow rates with varied liquid–gas velocity ratio

The flow flux ratio and the location may be adjusted independently to agree with specified characteristics of a given system. To have a better understanding of the combined effect of the local wetting efficiency and dynamic holdup, the ratio of the liquid to gas velocities at each radial section is varied from the previous case by switching the liquid inlet positions of high flow rate and low flow rate. As shown in Fig. 9, no radial flow is considered.

With a high liquid flow rate and low gas flow rate, the radial sections 4 and 5 possess a higher solid–liquid contact and dynamic liquid holdup than the other sections. In contrast, lower solid–liquid contact and dynamic liquid holdup are present in the radial sections 9 and 10 than in the rest of the sections. As exhibited in Fig. 10a, it is clear that the level of temperature rise was shifted with the switch of the liquid inlet positions. The level of benzene conversion rate across the reactor is also shifted with the corresponding temperature change shown in Fig. 10b. In the high liquid flow sections ($1.2U_{L,0}$) of Figs. 10a and 8a, the axial distance through which cell temperature reaches the maximum value was shorter with a lower gas flow

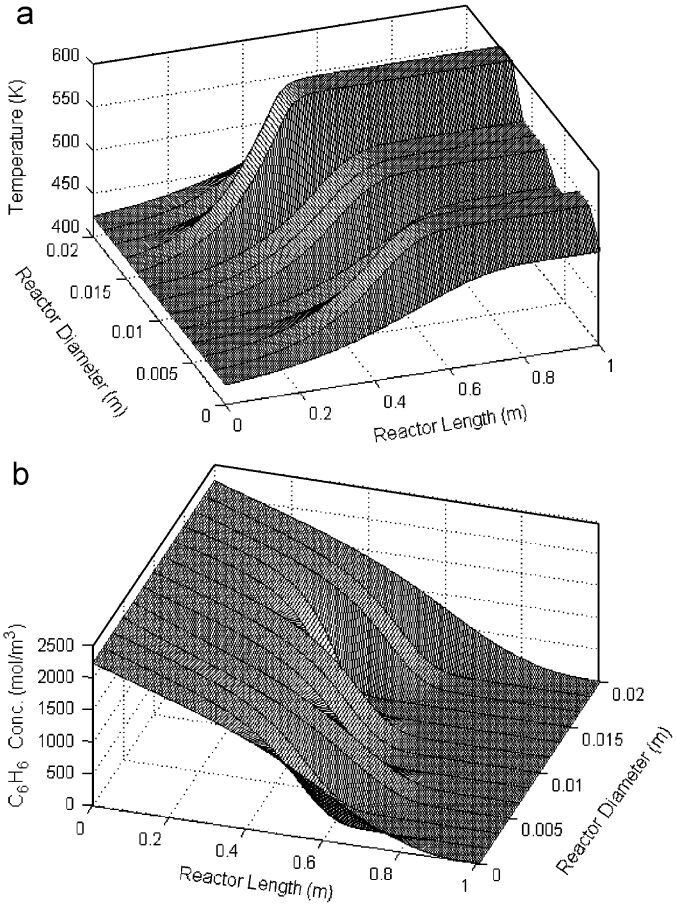

Fig. 10. 2D temperature profile (a) and benzene concentration profile (b). Unevenly distributed feed rate at reactor inlet, with varied ratio of $U_{L,0}/U_{G,0}$ at specified inlet locations. No radial flow distribution.

($0.8U_{G,0}$) than with a higher gas flow ($1.2U_{G,0}$). With the same high liquid velocity ($1.2U_{L,0}$), the phase transition was delayed due to the higher liquid holdup under weaker gas flow, while cell temperature builds up faster because less gas mass flow is available to carry out the reaction heat, as seen in the comparison between Figs. 10a and 8a. On the other hand, in the low liquid flow section ($0.8U_{L,0}$), the path reaching the maximum temperature is longer when the gas velocity is larger ($1.2U_{G,0}$), as reaction heat is removed faster with higher gas velocity. Even though lower dynamic liquid buildup due to larger gas velocity

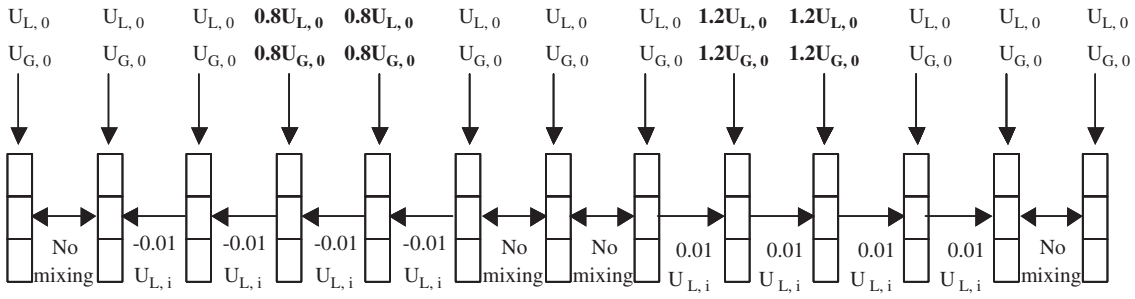

Fig. 11. Radial flow distribution exists between specified radial cell columns. Unevenly distributed feed rate at reactor inlet, with same ratio of $U_{L,0}/U_{G,0}$ at every inlet cell. Reaction conditions as given in case 2. Thirteen radial cell columns.

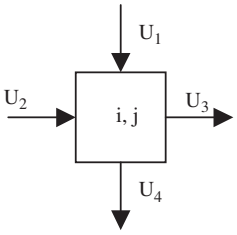

Fig. 12. Velocity diagram for the specified cell (i, j).

was expected to be beneficial for enhanced drying and reaction process, as well as the accelerated rate of temperature rise, the predicted temperature profile revealed a marginal effect of dynamic liquid holdup. In contrast, varied wetting efficiency due to changed liquid velocity was dominant in controlling the reaction rate and temperature rise.

5.4. Radial flow with perturbed inlet conditions

In this case, model simulation is focused on communication between cells in sustaining and promoting the local hot spot, as several distinct hot regions may co-exist and interact. A group of cells could be arranged so that heat and mass transfer processes between cells could be examined. As seen in Fig. 11, radial flow is added to the previous case of perturbed inlet conditions with a constant liquid–gas velocity ratio. A radial distribution in liquid flow over the catalyst without a corresponding change in gaseous reactant is a possible scenario for a local hot spot to migrate. Fig. 12 is given to illustrate the radial flow distribution. For example, we can have for liquid phase in specified cell (i, j),

$$U_2 = U_3 = -0.01U_1 \text{ for cell } (i, 3) \text{ to cell } (i, 5) \text{ (3 cells in each layer)},$$

$$U_2 = U_3 = 0.01U_1 \text{ for cell } (i, 9) \text{ to cell } (i, 11) \text{ (3 cells in each layer)},$$

where U_1 is the liquid velocity at the cell inlet.

The distributions of temperature and benzene concentration in the reactor are plotted in Figs. 13a and b, respectively. This simulation reveals a sensitive interplay between the exothermic reaction and the endothermic vaporization, coupled with

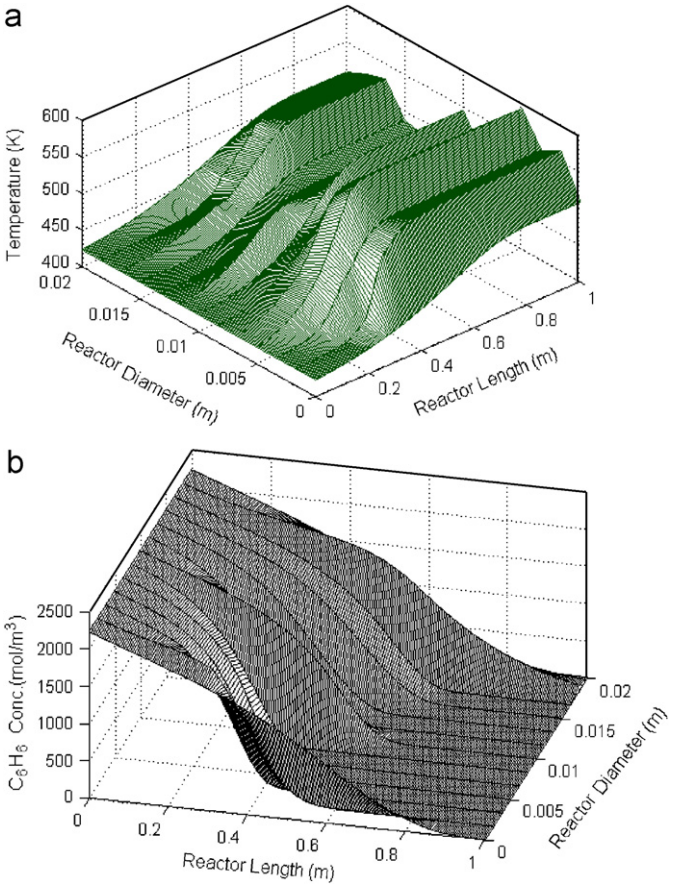

Fig. 13. 2D temperature profile (a) and benzene concentration profile (b). Radial flow distribution exists between specified radial cell columns. Unevenly distributed feed rate at reactor inlet, with same ratio of $U_{L,0}/U_{G,0}$ at every inlet cell.

the mass transport process and radial velocity distribution. Reactants entering the affected low flow region were converted at a rate greater than those in the surrounding region. The formation of dry spots by vaporization led to both a higher energy release and temperature. As the reactants passed out of the low flow region, they eventually mixed with the cooler reactants from the surrounding cells of the bed where the heat is dissipated. The heat flux along the radial direction to the surrounding cells increased the liquid component vapor

pressures and therefore increased the overall driving force for mass transport. For the high liquid flow region, the cooler liquid continually mixed laterally with the adjacent bed. Eventually, the other region was reached and the temperature profile crested. Hence, in this case, the radial flow and species exchange were beneficial to the expansion of the hot spot, while lowering its maximum temperature.

By changing the radial flow profile, the model can be used to either estimate the size and severity of the region based on measured temperature profiles or to understand the flow distribution given the size and severity of the region. In fact, in a commercial fixed bed reactor, a hot spot once formed may not stay constant afterward. Migration of hot spot may occur with small extent of lateral mixing or variation of flow field. The proposed modeling scheme can be applied repeatedly with a group of known flow frame to capture the relocation of hot spot.

5.5. Combination with CFD model

For the model to acquire complete predictive capabilities, it is worthwhile to compute the flow field explicitly to provide gas and liquid local flows, instead of adopting the user specified values as in the previous cell models. The computational fluid dynamics (CFD) simulation turns out to be a powerful tool to predict the macroscale non-reactive flow distribution, especially when the structure heterogeneity of the packed bed is accounted for.

For the reactive flow, the performance of multiphase reactors in principle can be predicted by solving simultaneously the conservation equations for mass, momentum and energy in combination with the constitutive equations for species transport, chemical reaction and phase transition. However, with multiple reactions and strong reaction heat generation which generally exists in the petrochemical industry, the current reactive CFD application still needs improvement to give satisfactory results. Since the general reactive CFD simulation is conducted for the whole computational domain (the whole reactor) and tends to track all reactions and hydrodynamics in a parallel approach, it is not easy to identify the reason for any numerical difficulty encountered when reaction kinetics is highly coupled and nonlinear, or when reactions are highly exothermic.

An alternative solution scheme could be combining the non-reactive CFD model with the mixing-cell reaction network model. In fact, to evaluate the impact of flow distribution on the performance of packed-bed reactors for an isothermal reaction with linear kinetics, CFD model results of the multiphase flow distribution were used as input information to a mixing-cell network model (Jiang et al., 2005). The preliminary results have shown promise that such solution scheme is capable of providing the information on the distribution of species concentrations for multiphase flow and simple isothermal reaction in packed beds. For a complex reaction system with non-isothermal chemical reactions and multi-component transport, a number of iterations of the sequential approach are necessary to update the temperature distribution. The non-reactive CFD simulation, at first, gives the flow velocity based on the bed heterogeneity and the known bed temperature. Then the cell network model is used to predict the temperature change within each cell. Such temperature distribution in each cell could be input to the non-reactive CFD simulation to update the flow velocity profile; in turn the temperature profile will be once again updated based on the cell network model. The iteration continues until the convergence criterion is met. Therefore, valuable for the purpose of diagnostic analysis of the operating commercial units, the proposed sequential approach is designed to bridge the gap between the CFD simulation and the complex reaction system.

6. Conclusion

This model was based on a network of perfectly stirred tanks. The first part of this paper was mainly concerned with validating the 1D model as a primary representation of the packed bed against experiment data. Each cell was established to incorporate the contribution of multiphase mass transfer, reaction kinetics, heat transfer and vaporization effects. The developed 1D model was proven to possess the capability to assess the effect of various parameters on reactor axial temperature profiles.

Once the model was established as a predictive tool, it was extended to cover the behavior of 2D systems. The 2D model exhibited how radial flow and change of inlet flow rates could affect the temperature map and lead to excessive temperatures in some reactor zones. Liquid flow rate, partial catalyst wetting and phase transition have significant effects on local hot spot formation. The novel mixing cell network approach based on the novel solution scheme was shown to be suitable and efficient for tracking temperature runaway in packed beds. Although purely theoretical in nature, the cell network model could be applied to important engineering activity, such as scale up of packed bed reactors. The model accounts for the various factors which change with the dimensions of a fixed bed, so that some of the experimental steps in scale up might be avoided. Most importantly, the model is designed to determine boundaries for safe operation and to prevent temperature runaways. To become fully predictive the model construction would need to be continued in linking CFD predictions for flow distribution with the cell network model for reactor performance assessment. A sequential modeling scheme is suggested as a plausible engineering approach, particularly helpful for systems in which the flow distribution is significantly affected by complex reactions. The future work could cover the experimental measurements of 2D flow map and corresponding temperature profiles, when the equipments and methods are available. Then the prediction of 2D model will be verified against the collected experimental data for the conditions studied.

Notation

a_{GL}	gas–liquid interphase area per unit reactor bed volume, m^2/m^3
a_{LS}	wetted catalyst area per unit reactor bed volume, m^2/m^3

A_w	bed-to-wall heat transfer area, m^2
c_p	specific heat capacity of gas or liquid, J/mol K
$C_{k,e}=C_{k,G}/He_k$	hypothetical concentration of liquid in equilibrium with bulk gas for species k, mol/m^3
$C_{k,G}$	concentration of species k in gas, mol/m^3
$C_{k,GS}$	concentration of species k on the dry side of catalyst, mol/m^3
$C_{k,L}$	concentration of species k in liquid, mol/m^3
$C_{k,LS}$	concentration of liquid species k on the wetted catalyst surface, mol/m^3
D_{eff}	effective volumetric diffusion coefficient, m^2/s
D_m	molecular diffusivity, m^2/s
F_G	molar gas flux, mol/m^2 s
$\Delta H_{f,G}$	standard enthalpy of formation for gas compound at 298.15 K, kJ/mol
ΔH_R	heat of reaction, kJ/mol
ΔH_T	enthalpy of species formation at temperature T, kJ/mol
ΔH_v	enthalpy difference between gas and liquid at temperature T, kJ/mol
He_k	Henry's law constant of solubility for species k
k_{GS}	gas–solid mass transfer coefficient, m/s
$k_L a_{GL}$	liquid side mass transfer coefficient for gas to flowing liquid, 1/s
k_{LS}	liquid–solid mass transfer coefficient, m/s
k_{p0}, k_{p1}, k_{p2}	Arrhenius prefactors of heterogeneous reaction rate constant
$K_L a_{GL}$	overall volumetric mass transfer coefficient from gas to flowing liquid, 1/s
L_c	cell length or the length of control volume, m
M_T	Thiele modulus
P	pressure, atm
Q_w	bed-to-wall heat loss, kJ/m^3 s
r_L	intrinsic reaction rate for liquid phase, mol/m^3 s
R	gas constant, kJ/kmol K
R_G	apparent reaction rate for gas phase, mol/m^3 s
T	temperature inside the cell and at the cell outlet, K
T_{in}	initial temperature, K
T_w	wall temperature, K
U_G	gas superficial velocity, m/s
U_L	liquid superficial velocity, m/s
U_w	bed-to-wall heat transfer coefficient, kJ/m^2 K s
V_c	control volume, m^3
z	axial coordinate

Greek letters

ε_B	bed porosity
η_{CE} $= 1.617 Re_L^{0.146} Ga_L^{-0.0711}$	external catalyst wetting efficiency
η_0	catalyst effectiveness factor for liquid phase reaction
v_k	stoichiometric coefficient for species k
ρ	phase density, kg/m^3
ϕ	species concentration at cell inlet
ψ	temperature at the cell inlet, K

Sub/superscripts

e	equilibrium
G	gas phase
in	cell inlet
k	species number
L	liquid phase
out	cell outlet
S	solid phase
v	phase vaporization
w	reactor wall
0	input
1	hydrogen, H_2
2	benzene, C_6H_6
3	cyclohexane, C_6H_{12}

Acknowledgments

The authors would like to thank Dr. P.A. Ramachandran and Dr. M.P. Dudukovic at Washington University in St. Louis for valuable discussions and constructive comments.

References

Chaudhari, R.V., Jaganathan, R., Mathew, S.P., Julcour, C., Delmas, H., 2002. Hydrogenation of 1,5,9-cyclododecatriene in fixed-bed reactors: down vs. upflow modes. A.I.Ch.E. Journal 48, 110.

Cheng, Z.M., Yuan, W.K., 2002. Influence of hydrodynamic parameters on performance of a multiphase fixed-bed reactor under phase transition. Chemical Engineering Science 57, 3407.

Cheng, Z.M., Abdulhakeim, M.A., Yuan, W.K., 2001. Intensification of phase transition on multiphase reactions. A.I.Ch.E. Journal 47, 1185.

Deans, H.A., Lapidus, L., 1960. A computational model for predicting and correlating the behavior of fixed-bed reactors: 1. Derivation of model for nonreactive systems. A.I.Ch.E. Journal 6, 656–663.

Dwivedi, P.N., Upadhyah, S.N., 1977. Particle-fluid mass transfer in fixed and fluidized beds. Industrial Engineering Chemistry Process Design and Development 16, 157.

Ellman, M.J., Midoux, N., Wild, G., Laurent, A., Charpentier, J.C., 1990. A new improved liquid hold-up correlation for trickle-bed reactors. Chemical Engineering Science 45, 1677–1684.

Fukushima, S., Kusaka, K., 1977. Liquid-phase volumetric and mass-transfer coefficient, and boundary of hydrodynamic flow region in packed column with cocurrent downward flow. Journal of Chemical Engineering of Japan 10, 468.

Guo, J., Al-Dahhan, M., 2004. A sequential approach to modeling catalytic reactions in packed bed reactors. Chemical Engineering Science 59, 2023.

Haure, P.M., Hudgins, P.R., Silveston, P.L., 1989. Periodic operation of a trickle-bed reactor. A.I.Ch.E. Journal 35, 1437.

Jaffe, S.B., 1976. Hot spot simulation in commercial hydrogenation processes. Industrial Engineering Chemistry Process Design and Development 15, 410–416.

Jiang, Y., Guo, J., Al-Dahhan, M., 2005. Multiphase flow packed bed reactor modeling: combining CFD and cell network model. Industrial Engineering Chemistry Research 44, 4940–4948.

Kufner, R., Hofmann, H., 1990. Implementation of radial porosity and velocity distribution in a reactor model for heterogeneous catalytic gas phase reactions (TORUS-Model). Chemical Engineering Science 45, 2141–2146.

Levenspiel, O., 1996. The Chemical Reactor Omnibook. OSU Book Stores, Corvallis, Oregon.

Mao, Z.S., Xiong, T.Y., Chen, J.Y., 1993. Theoretical prediction of static liquid holdup in trickle bed reactors and comparison with experimental results. Chemical Engineering Science 48, 2697.

Perry, R.H., Green, D.W., 1997. Perry's Chemical Engineers' Handbook, seventh ed. McGraw-Hill, New York.

Ramachandran, P.A., Chaudhari, R.V., 1983. Three-phase Catalytic Reactors. Gordon and Breach Science Publishers, New York.

Ronze, D., Fongarland, P., Pitault, I., Forissier, M., 2002. Hydrogen solubility in straight run gasoil. Chemical Engineering Science 57, 547–555.

Schnitzlein, K., Hofmann, H., 1987. An alternative model for catalytic fixed bed reactors. Chemical Engineering Science 42, 2569–2577.

Snijder, E.D., Versteeg, G.F., van Swaaij, W.P.M., 1994. Some properties of $LaNi_{5-x}Al_x$ metal alloys and the diffusion coefficient and solubility of hydrogen in cyclohexane. Journal of Chemical and Engineering Data 39, 405–408.

Specchia, V., Baldi, G., 1979. Heat transfer in trickle-bed reactors. Chemical Engineering Communications 3, 483–499.

Tan, C.S., Smith, J.M., 1980. Catalyst particle effectiveness with unsymmetrical boundary conditions. Chemical Engineering Science 35, 1601.

Watson, P.C., Harold, M.P., 1993. Dynamic effects of vaporization with exothermic reaction in a porous catalytic pellet. A.I.Ch.E. Journal 39, 989–1006.

Yaws, C.L., 1999. Chemical Properties Handbook. McGraw-Hill, New York.

Zhou, Z.M., Cheng, Z.M., Yuan, W.K., 2005. Simulating a multiphase reactor with continuous phase transition. Chemical Engineering Science 60, 3207–3215.